

The Potential Energy Surface of BH₅ and the Rate of the Hydrogen Scrambling

Kyung Hyun Kim and Yongho Kim*

Department of Chemistry and Institute of Natural Sciences, Kyung Hee University,

Yongin-City, Kyunggi-Do 449-701, Korea

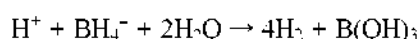
Received March 4, 2003

The BH₅ molecule, which is suggested as an intermediate of the acidolysis of BH₄⁻, contains a weak two-electron-three-center bond and it requires extremely high-level of theories to calculate the energy and structure correctly. The structures and energies of BH₅ and the transition state for the hydrogen scrambling have been studied using recently developed multi-coefficient correlated quantum mechanical methods (MCCMs). The dissociation energies and the barrier heights agree very well with the previous results at the CCSD(T)/TZ(3d1f1g, 2p1d) level. We have also calculated the potential energy curves for the dissociation of BH₅ to BH₃ and H₂. The lower levels of theory were unable to plot correct potential curves, whereas the MCCM methods give very good potential energy curves and requires much less computing resources than the CCSD(T)/TZ(3d1f1g, 2p1d) level. The potential energy of the BH₅ scrambling has been obtained by the multiconfiguration molecular mechanics algorithm (MCMM), and the rates are calculated using the variational transition state theory including multidimensional tunneling approximation. The rate constant at 300 K is $2.1 \times 10^9 \text{ s}^{-1}$, and tunneling is very important.

Key Words : BH₅, Hydrogen scrambling, MCMM, Rate constant

Introduction

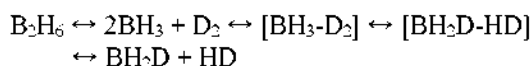
The existence of BH₅ was postulated on the basis of experimental observations of the acidolysis of BH₄⁻ in aqueous solution.¹



In acidic H₂O, BH₄⁻ accepts a proton to form BH₅, which is dissociated into BH₃ and H₂.



The first step is slow and the dissociation is known to be very fast. In D₂O, mostly HD molecules are formed from the same mechanism as above, but a small amount of H₂ is also detected. In basic D₂O, the unreacted BH₄⁻ turned into, first BH₃D⁻, then BH₂D₂⁻, etc.² Pitzer *et al.* have reported that B₂D₆ was obtained by shaking B₂H₆ with D₂ at room temperature.³ The possible mechanism is as following.



These observations suggest the existence of BH₅ and the scrambling of hydrogens. Later, BH₅ has been detected spectroscopically in a low temperature matrix.⁴

Schreiner *et al.* have performed extensive *ab initio* calculations for the BH₅ systems.⁵ They found that geometry and energy of BH₅ depend very much on the level of theory and the size of basis sets. The HF level of theory is inadequate for BH₅, and even CCSD(T) level with the DZP basis sets cannot predict the structure of BH₅ correctly. BH₅ should be considered as a molecule with chemical bonds between BH₃ and H₂.⁵ This is a weak 2-electron-3-center bond, and the correct description for the bond dissociation

can be a critical test for theory. Based on the comparison between the dissociation energy of BH₅ into BH₃ and H₂ and the barrier height for the scrambling, Schreiner *et al.* have concluded that the hydrogen scrambling is not likely. They have also pointed out the possibility of large tunneling effect. Therefore it is necessary to calculate the scrambling rate and the role of tunneling to explain the experimental observations correctly.

Since the reliable *ab initio* calculations for BH₅ require very high levels of electron correlation with large basis sets, it is almost impractical to generate good potential energy surface for the rate calculation. We have used recently developed multi-coefficient corrected quantum mechanical methods (MCCM) and the multi-configuration molecular mechanics method (MCMM) to generate potential energy surface, and calculated rates using the variational transition state theory including multidimensional tunneling approximations.

Computational Methods

All electronic structure calculations were performed with the *Gaussian 98* program packages.⁶ Initial geometries for BH₅ complex were fully optimized at the QCISD level of theory with the TZ2P basis sets, and then the structures of BH₅ complex were partially optimized by fixing the distance between Boron and the center of H₂ along the dissociation coordinate of BH₅ to BH₃ and H₂. The MCCM potential energy curves were calculated using these partially optimized structures. The full geometry optimization was also performed, and frequencies and zero-point energies for H₂, BH₃, and BH₅ were obtained using the optimized structures. The structures optimized at the QCISD/TZ2P level has been used

for the potential energy curve at the G3 level. Although we followed the G3 procedures, it is not the real G3, since the G3 level uses the MP2/6-31G(d) method for the geometry optimization. Therefore we will denote it as G3//QCISD/TZ2P. For the potential energy curve for BH₃ dissociation, the single-point MCCM calculations were performed using the structures partially optimized at the QCISD/TZ2P level. So these calculations are denoted as MCCM//QCISD/TZ2P.

All of the multi-coefficient correlated quantum mechanical methods have been described elsewhere in detail,⁷⁻¹¹ therefore, only a short description of each method employed will be given here. Since all of these methods involve differences between energies at different basis sets and theory levels, a short notation has been used in order to write the equation for a multilevel energy succinctly. In this notation, the pipe “|” is used to represent the energy difference either between two one-electron basis sets *B1* and *B2* or between two levels of electronic structure theory *L1* and *L2*, e.g., Moller-Plesset second-order perturbation theory and Hartree-Fock theory. The energy difference between two basis sets is represented as

$$\Delta E(L/B2|B1) = E(L/B2) - E(L/B1) \quad (1)$$

where *L* is a particular electronic structure method, and *B1* is smaller than *B2*. The energy change that occurs upon improving the treatment of the correlation energy is represented by

$$\Delta E(L2|L1/B) = E(L2/B) - E(L1/B) \quad (2)$$

where *L1* is a lower level of theory than *L2*, and *B* is a common one-electron basis set. Finally, the change in energy increment due to increasing the level of the treatment of the correlation energy with one basis set as compared to the increment obtained with a smaller basis set is represented as

$$\begin{aligned} \Delta E(L2|L1/B2|B1) \\ = E(L2/B2) - E(L1/B2) - [E(L2/B1) - E(L1/B1)] \end{aligned} \quad (3)$$

The Utah variant of MCCM (MCCM-UT-L) methods are written as

$$\begin{aligned} E(\text{MCCM-UT-L}) = & c_1 E(\text{HF/cc-pVDZ}) \\ & + c_2 \Delta E(\text{HF/cc-pVTZ|cc-pVDZ}) \\ & + c_3 \Delta E(\text{MP2|HF/cc-pVDZ}) \\ & + c_4 \Delta E(\text{MP2|HF/cc-pVTZ|cc-pVDZ}) \\ & + c_5 \Delta E(L|\text{MP2/cc-pVDZ}) + E_{\text{SO}} + E_{\text{CC}} \end{aligned} \quad (4)$$

where *L* is either MP4SDQ or CCSD. Equations for the electronic energies for the multi-coefficient Gaussian-3 (MCG3)⁹ and the multi-coefficient QCISD (MC-QCISD)¹¹ methods are given below.

$$\begin{aligned} E(\text{MCG3}) = & c_1 E(\text{HF/6-31G}(d)) \\ & + c_2 \Delta E(\text{HF/MG3|6-31G}(d)) \\ & + c_3 \Delta E(\text{MP2|HF/6-31G}(d)) \\ & + c_4 \Delta E(\text{MP2|HF/MG3|6-31G}(d)) \\ & + c_5 \Delta E(\text{MP4SDQ|MP2/6-31G}(d)) \\ & + c_6 \Delta E(\text{MP4SDQ|MP2/6-31G}(2df,p)|6-31G}(d)) \\ & + c_7 \Delta E(\text{MP4|MP4SDQ/6-31G}(d)) \end{aligned}$$

$$+ c_8 \Delta E(\text{QCISD}(T)|\text{MP4/6-31G}(d)) + E_{\text{SO}} + E_{\text{CC}} \quad (5)$$

$$\begin{aligned} E(\text{MC-QCISD}) = & c_1 E(\text{HF/6-31G}(d)) \\ & + c_2 \Delta E(\text{MP2|HF/6-31G}(d)) \\ & + c_3 \Delta E(\text{MP2/MG3|6-31G}(d)) \\ & + c_4 \Delta E(\text{QCISD|MP2/6-31G}(d)) \end{aligned} \quad (6)$$

The MG3 (modified G3) basis set denotes the G3 large basis set without the core polarization functions.¹² Each of these methods assigns coefficients to each energy difference involved in the linear combination; the coefficients have been optimized to fit the atomization energies of 82 molecules containing first-and-second-row elements.¹³ In the MCCM-UT, MC-QCISD, and MCG3 methods, the basis set deficiency has been corrected by the linear combination of the energy difference with optimized coefficients.

The multilevel structure, energy, and Hessian are calculated by using the MULTILEVEL 2.1.1 program.¹⁴ This program uses the GAUSSIAN 98 package to obtain the energy, gradient, and Hessian components and then combines the components to calculate the multilevel energy, gradient, and Hessian. Frequencies were calculated from the Hessian. Single-level Hessians were used with the NewtonRaphson step. In most cases, an HF/6-31G(d,p) Hessian was recalculated every three steps, and this matrix was used in the determination of every Newton-Raphson step for all MULTILEVEL optimizations.

Details of the multiconfiguration molecular mechanics (MCMM) algorithm have been described elsewhere in detail;¹⁵ therefore, only a brief description of each method employed will be given here. In the MCMM formalism, the reactive system can be defined by using several valence bond configurations or, more generally, diabatic configurations corresponding to each of the minima on the potential energy surface. Each configuration can be described by a molecular mechanics potential, $V_{11}(\mathbf{q})$ and $V_{22}(\mathbf{q})$, which is correct in the vicinity of the well. For a geometry \mathbf{q} far from the minima the energy can be expressed in terms of the two diabatic configurations by solving the secular equation:

$$\begin{vmatrix} V_{11} - V & V_{12} \\ V_{12} & V_{22} - V \end{vmatrix} = 0 \quad (7)$$

where the term $V_{12}(\mathbf{q})$ is called the resonance energy function or resonance integral, and V denotes the lowest-energy eigenvalue of \mathbf{V} . The element V_{ij} of the matrix \mathbf{V} may be considered to be the representation of the electronic Hamiltonian (including nuclear repulsion) in an electronically diabatic basis, and the eigenvalue V is the expectation value of the electronic Hamiltonian (including nuclear repulsion) for the lowest-energy electronically adiabatic state. This eigenvalue is given by

$$\begin{aligned} V(\mathbf{q}) = & \frac{1}{2} \{ (V_{11}(\mathbf{q}) + V_{22}(\mathbf{q})) \\ & - [(V_{11}(\mathbf{q}) - V_{22}(\mathbf{q}))^2 + 4V_{12}(\mathbf{q})^2]^{1/2} \}, \end{aligned} \quad (8)$$

the components of its gradient are given by

$$g_i = \left(\frac{\partial V}{\partial q_i}\right) = \frac{1}{2} \left\{ \left(\frac{\partial V_{11}}{\partial q_i}\right) + \left(\frac{\partial V_{22}}{\partial q_i}\right) - \left[\frac{4V_{12} \left(\frac{\partial V_{12}}{\partial q_i}\right) + [V_{11} - V_{22}] \left[\left(\frac{\partial V_{11}}{\partial q_i}\right) - \left(\frac{\partial V_{22}}{\partial q_i}\right) \right]}{[(V_{11} + V_{22})^2 + 4V_{12}^2]^{1/2}} \right] \right\} \quad (9)$$

and the elements of its Hessian are given by

$$f_{ij} = \left(\frac{\partial^2 V}{\partial q_i \partial q_j}\right) = \frac{1}{2} \left\{ \left(\frac{\partial^2 V_{11}}{\partial q_i \partial q_j}\right) + \left(\frac{\partial^2 V_{22}}{\partial q_i \partial q_j}\right) + \left[\frac{4V_{12} \left(\frac{\partial V_{12}}{\partial q_i}\right) + (V_{11} - V_{22}) \left[\left(\frac{\partial V_{11}}{\partial q_i}\right) - \left(\frac{\partial V_{22}}{\partial q_i}\right) \right]}{[(V_{11} - V_{22})^2 + 4V_{12}^2]^{3/2}} \right] \times \left[\frac{4V_{12} \left(\frac{\partial V_{12}}{\partial q_j}\right) + (V_{11} - V_{22}) \left[\left(\frac{\partial V_{11}}{\partial q_j}\right) - \left(\frac{\partial V_{22}}{\partial q_j}\right) \right]}{[(V_{11} - V_{22})^2 + 4V_{12}^2]^{1/2}} \right] - \left[\frac{4 \left(\frac{\partial V_{12}}{\partial q_i}\right) \left(\frac{\partial V_{12}}{\partial q_j}\right) + \left[\left(\frac{\partial V_{11}}{\partial q_i}\right) - \left(\frac{\partial V_{22}}{\partial q_i}\right) \right] \left[\left(\frac{\partial V_{11}}{\partial q_j}\right) - \left(\frac{\partial V_{22}}{\partial q_j}\right) \right]}{[(V_{11} - V_{22})^2 + 4V_{12}^2]^{1/2}} - \left[\frac{4V_{12} \left(\frac{\partial^2 V_{12}}{\partial q_i \partial q_j}\right) + (V_{11} - V_{22}) \left[\left(\frac{\partial^2 V_{11}}{\partial q_i \partial q_j}\right) - \left(\frac{\partial^2 V_{22}}{\partial q_i \partial q_j}\right) \right]}{[(V_{11} - V_{22})^2 + 4V_{12}^2]^{1/2}} \right] \right\} \quad (10)$$

Note that V tends to the energy V_{11} of configuration 1 (reactants) or the energy V_{22} of configuration 2 (products) whenever the value of the resonance integral is negligible. The critical issue in the MCMM formulation is the calculation of that resonance integral and its derivatives, since the V_{11} and V_{22} terms and their derivatives are extracted from the molecular mechanics force field. Note that V_{11} is generated using the connectivity (valence structure) of reactants, and V_{22} is generated using the connectivity of products.

From Eq. (7), $V_{12}(\mathbf{q})$ can be expressed as:

$$V_{12}(\mathbf{q})^2 = [V_{11}(\mathbf{q}) - V(\mathbf{q})][V_{22}(\mathbf{q}) - V(\mathbf{q})] \quad (11)$$

Near the arbitrary geometry $\mathbf{q}^{(k)}$, each quantity on the right hand side of Eq. (11) can be expanded in Taylor's series. Thus,

$$V(\mathbf{q}; k) \cong V^{(k)} + \mathbf{g}^{(k)\top} \cdot \Delta \mathbf{q}^{(k)} + \frac{1}{2} \Delta \mathbf{q}^{(k)\top} \cdot \mathbf{f}^{(k)} \cdot \Delta \mathbf{q}^{(k)} \quad (12)$$

where

$$\Delta \mathbf{q}^{(k)} = \mathbf{q} - \mathbf{q}^{(k)} \quad (13)$$

and $V^{(k)}$, $\mathbf{g}^{(k)}$, and $\mathbf{f}^{(k)}$ are the target energy, gradient, and Hessian matrix respectively of the reference point (note that

if the reference geometry corresponds to a saddle point or local minimum (well) on the potential energy hypersurface, $\mathbf{g}^{(k)}$ is zero). Furthermore we expand the diagonal elements of V_{nn} around the geometry $\mathbf{q}^{(k)}$:

$$V_{nn}(\mathbf{q}; k) \cong V_n^{(k)} + \mathbf{g}_n^{(k)\top} \Delta \mathbf{q} + \frac{1}{2} \Delta \mathbf{q}^\top \mathbf{f}_n^{(k)} \Delta \mathbf{q} \quad (14)$$

where

$$V_n^{(k)} = V_{nn}(\mathbf{q}^{(k)}), \quad \mathbf{g}_n^{(k)} = \left(\frac{\partial V_{nn}}{\partial \mathbf{q}}\right)_{\mathbf{q} = \mathbf{q}^{(k)}},$$

$$\mathbf{f}_n^{(k)} = \left(\frac{\partial^2 V_{nn}}{\partial \mathbf{q} \partial \mathbf{q}}\right)_{\mathbf{q} = \mathbf{q}^{(k)}} \quad (15)$$

for $n = 1, 2$. Note that the quantities with superscript (k) are constants evaluated at the geometry $\mathbf{q}^{(k)}$ of each reference point, k , and therefore are independent of \mathbf{q} . The quantities V_{nn} defined in Eq. (14) and $V_{12}(\mathbf{q}; k)$ and its derivatives are functions dependent on the geometry, \mathbf{q} , as well as on the geometry of the reference point k . Substituting Eqs. (12) and (14) into (11), we obtain the following general form of the V_{12} term:

$$V_{12}(\mathbf{q}; k)^2 \cong (V_1^{(k)} - V^{(k)})(V_2^{(k)} - V^{(k)}) + (V_2^{(k)} - V^{(k)})(\mathbf{g}_1^{(k)} - \mathbf{g}^{(k)})^\top \Delta \mathbf{q} + (V_1^{(k)} - V^{(k)})(\mathbf{g}_2^{(k)} - \mathbf{g}^{(k)})^\top \Delta \mathbf{q} + \frac{1}{2} (V_2^{(k)} - V^{(k)}) \Delta \mathbf{q}^\top (\mathbf{f}_1^{(k)} - \mathbf{f}^{(k)}) \Delta \mathbf{q} + \frac{1}{2} (V_1^{(k)} - V^{(k)}) \Delta \mathbf{q}^\top (\mathbf{f}_2^{(k)} - \mathbf{f}^{(k)}) \Delta \mathbf{q} + [(\mathbf{g}_1^{(k)} - \mathbf{g}^{(k)})^\top \Delta \mathbf{q}][(\mathbf{g}_2^{(k)} - \mathbf{g}^{(k)})^\top \Delta \mathbf{q}] \quad (16)$$

Equation 16 provides an analytic expression for evaluating the resonance integral in the vicinity of a reference point. However, when dealing with a nuclear configuration far from the reference point k , the value $V_{12}(\mathbf{q}; k)$ given by Eq. (16) is unbounded either positive or negative, and hence the value of $V(\mathbf{q})$ given by Eq. (8) diverges. In this paper, we applied a modified version of a Shepard interpolation scheme^{16,17} previously applied directly to $V(\mathbf{q})$. This method does not make any assumption, and it allows for systematic improvement as the number M of points k is increased.

The Shepard interpolation algorithm, in internal coordinates \mathbf{q} , yields

$$V_{12}^S(\mathbf{q}) = \sum_{k=1}^M W_k(\mathbf{q}) V_{12}'(\mathbf{q}; k) \quad (17)$$

where the normalized weights $W_k(\mathbf{q})$ are defined as

$$W_k(\mathbf{q}) = \frac{w_k(\mathbf{q})}{w(\mathbf{q})} \quad (18)$$

and

$$w(\mathbf{q}) = \sum_{l=1}^M w_l(\mathbf{q}) \quad (19)$$

and $V_{12}'(\mathbf{q};k)$ is a modified quadratic function

$$[V_{12}'(\mathbf{q};k)]^2 = [V_{12}(\mathbf{q};k)]^2 u(\mathbf{q};k) \quad (20)$$

where the quadratic part is

$$[V_{12}(\mathbf{q};k)]^2 = D^{(k)} \left[1 + \mathbf{b}^{(k)\top} (\mathbf{q} - \mathbf{q}^{(k)}) + \frac{1}{2} (\mathbf{q} - \mathbf{q}^{(k)})^\top \mathbf{C}^{(k)} (\mathbf{q} - \mathbf{q}^{(k)}) \right] \quad (21)$$

and the modification is

$$u(\mathbf{q};k) = \begin{cases} \exp(-\delta/[V_{12}(\mathbf{q};k)]^2), & [V_{12}(\mathbf{q};k)]^2 > 0 \\ 0, & [V_{12}(\mathbf{q};k)]^2 \leq 0 \end{cases} \quad (22)$$

We use a very small value of δ , $1 \times 10^{-8} E_h^2$ (where $1 E_h = 1$ hartree), so that Eq. (22) converges rapidly to 1 with increasing values of $[V_{12}(\mathbf{q};k)]^2$. The constants $D^{(k)}$, $\mathbf{b}^{(k)}$, and $\mathbf{C}^{(k)}$ are chosen such that Eq. (20) combined with Eq. (8) reproduces the expansion 12.

The weights should be chosen so that several conditions are fulfilled:

$$w_k(\mathbf{q}^{(k)}) = 1, \quad \text{all } k; \quad (23)$$

$$w_k(\mathbf{q}^{(k')}) \ll 1, \quad k' \neq k; \quad (24)$$

$$\left. \frac{\partial w_k}{\partial \mathbf{q}} \right|_{\mathbf{q} = \mathbf{q}^{(k')}} \equiv \mathbf{0}, \quad \text{all } k'; \quad (25)$$

$$\left. \frac{\partial^2 w_k}{\partial \mathbf{q}^2} \right|_{\mathbf{q} = \mathbf{q}^{(k')}} \equiv \mathbf{0}, \quad \text{all } k'. \quad (26)$$

Equations (23) and (24) are required so that Eqs. (8), (17), and (18) essentially reproduce the values of the target Born-Oppenheimer surface at the Shepard points. Eqs. (25) and (26) are required so that Eqs. (8), (17), and (18) reproduce the linear and quadratic terms of Eq. (12) at the Shepard points. In fact, w_k goes to zero as \mathbf{q} approaches $\mathbf{q}^{(k')}$, $k' \neq k$, and it must do so rapidly enough to preserve these linear and quadratic terms as well. Furthermore, $w_k(\mathbf{q})$ should be continuous and smooth, as we move from point k to point k' , the values of $V_{12}(\mathbf{q})$ and its derivatives should go smoothly from their values at $\mathbf{q}^{(k)}$ to their values at $\mathbf{q}^{(k')}$. The weighting function we are using is

$$w_k(\mathbf{q}) = \frac{[d_k(\mathbf{q})]^{-1}}{\sum_{i=1}^M \frac{1}{[d_i(\mathbf{q})]^{-1}}} \quad (27)$$

where $d_k(\mathbf{q})$ denotes a generalized distance between \mathbf{q} and $\mathbf{q}^{(k)}$ defined as:

$$d_k(\mathbf{q}) = \sqrt[4]{\sum_{i=1}^{N'} (q_i - q_i^{(k)})^2} \quad (28)$$

where N' is less than or equal to the number N of internal coordinates used in Eqs. (8)-(18).

The reaction rates have been calculated using the variational transition state theory including multidimensional tunneling approximation, which have also been described in many literatures.¹⁸⁻²⁰ We have used MC-Tinkerate that interconnect Polyrate and Tinker program packages for the rate calculations.

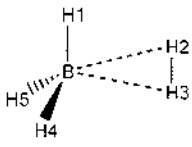
Results and Discussion

The optimized structures of BH_3 at the QCISD level have C_s symmetry. The MCCM level of theory also predicts the C_s structure and the geometrical parameters are listed in Table 1 along with the previous high-level *ab initio* results.⁵ The bond lengths for B-H2 and B-H3 at the QCISD level and are longer than the corresponding values from the *ab initio* study, whereas those from the MCCMs are slightly shorter. The geometrical parameters from the MCCMs show good agreement with those from the CCSD(T)/TZ(3d1f.2p1d) level. In particular, the structure from the MCG3 method agrees very well. Table 2 lists the geometrical parameters for the transition state (TS) of hydrogen scrambling. The QCISD level predict the TS structure with C_{2v} symmetry, which is consistent with the CCSD(T)/TZ(3d1f.2p1d) level. All MCCMs used in this study give the same symmetry for the TS too. The TS structures from the MCG3 and MC-QCISD methods agree almost perfectly with that from CCSD(T)/TZ(3d1f.2p1d) level.

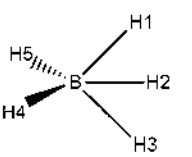
Table 3 lists the dissociation energies of BH_3 and barrier heights of hydrogen scrambling calculated at various levels of theory. The D_e values from the QCISD level are 2.14 and 1.89 kcal/mol, respectively, which are too small, and the V^\ddagger values are 7.52 and 7.57 kcal/mol, respectively. Schreiner *et al.*⁵ have performed various levels of *ab initio* calculations for the BH_3 systems. They found that geometry and energy of BH_3 depend very much on the level of theory and the size of basis sets. The D_e values at the CCSD(T) level with TZ2P and DZP basis sets were 3.32 and 0.82 kcal/mol, respectively. They have reported 5.82 and 5.65 kcal/mol for the D_e and V^\ddagger values, respectively, at the CCSD(T)/TZ(3d1f1g.2p1d)//CCSD(T)/TZ(3d1f.2p1d) level, which is the highest level of theory used so far. The D_e and V^\ddagger values at the CCSD(T)/TZ(3d1f.2p1d) level were 5.26 and 6.11 kcal/mol, respectively. Adding one set of boron g-type function increases the dissociation energy and decreases the barrier height. Considering higher electron correlation and using larger basis sets seem to increase the dissociation energy and decrease the barrier height.

All D_e and V^\ddagger values from the MCCM agree very well with those from the CCSD(T)/TZ(3d1f1g.2p1d) level. In particular, the MCCM-UT-CCSD values agree almost perfectly. The G3//QCISD/TZ2P level underestimates the dissociation energy and slightly overestimates the barrier height. The D_0 values at the CCSD(T)/TZ(3d1f1g.2p1d) level is 0.92 kcal/mol, which is larger than all the MCCM values. Schreiner *et al.* have obtained zero-point energies

Table 1. Geometrical parameters of BH₅ optimized at the MCCM levels along with the high level *ab initio* results^a

Parameters	QCISD/ TZ2P	MC-QCISD	MCCM-UT- CCSD	MCCM-UT- MP4SDQ	MCG3	CCSD(T)/TZ (3d1f,2p1d) ^b	
	$r(\text{B-H1})$	1.198	1.203	1.196	1.195	1.204	1.202
$r(\text{B-H2})$	1.472	1.401	1.401	1.397	1.411	1.422	1.422
$r(\text{B-H3})$	1.484	1.415	1.416	1.411	1.425	1.436	1.436
$r(\text{B-H4})$	1.191	1.194	1.187	1.186	1.195	1.194	1.194
$r(\text{H2-H3})$	0.786	0.808	0.796	0.796	0.805	0.799	0.799
$\theta(\text{H1-B-H2})$	80.2	79.2	79.5	79.5	79.4	79.6	79.6
$\theta(\text{H2-B-H3})$	30.8	33.4	32.8	32.9	33.0	32.5	32.5
$\theta(\text{H4-B-H5})$	119.9	120.1	120.0	120.1	120.1	120.1	120.1

^aBH₅ structure has C_s symmetry. Lengths are in Å and angles in degree. ^bReference 5.**Table 2.** Geometrical parameters for the transition state of hydrogen scrambling in BH₅ optimized at the MCCM levels along with the high level *ab initio* results^a

Parameters	QCISD/TZ2P	MC-QCISD	MCCM-UT- CCSD	MCCM-UT- MP4SDQ	MCG3	CCSD(T)/TZ (3d1f,2p1d) ^b	
	$r(\text{B-H1})$	1.268	1.268	1.260	1.258	1.271	1.270
$r(\text{B-H2})$	1.250	1.250	1.242	1.240	1.253	1.251	1.251
$r(\text{B-H4})$	1.180	1.187	1.181	1.178	1.187	1.187	1.187
$r(\text{H1-H2})$	1.080	1.089	1.081	1.080	1.088	1.088	1.088
$\theta(\text{H1-B-H2})$	50.8	51.2	51.2	51.2	51.0	51.0	51.0
$\theta(\text{H4-B-H5})$	128.1	128.1	128.1	128.1	128.0	128.1	128.1

The TS structure has C_{2v} symmetry. Lengths are in Å and angles in degree. ^bReference 5.**Table 3.** Dissociation energies of BH₅ and barrier height for hydrogen scrambling calculated at various levels of theory^a

Level	D _e	D ₀	D _e (fit)	V [‡]
CCSD+T(CCSD)/[5s4p3d1f/4s2p1d]/MP2/[3s2p1d/2s1p] ^b	5.4	0.9		7.2
CCSD(T)/TZ2P ^c	3.32	0.72		6.79
CCSD(T)/DZP ^c	0.89	0.19		6.38
CCSD(T)/TZ(3d1f,2p1d) ^f	5.26	0.36		6.11
CCSD(T)/TZ(3d1f1g,2p1d)/CCSD(T)/TZ(3d1f,2p1d) ^f	5.82	0.92		5.65
QCISD/TZ2P	2.14	-2.69		7.52
G3//QCISD/TZ2P	4.95		5.13	6.10
CCSD(T)/cc-pVQZ//QCISD/TZ2P	5.58		5.74	5.96
MC-QCISD	6.15	0.83	6.12	5.44
MCCM-UT-CCSD	5.76	0.37	5.76	5.71
MCCM-UT-MP4SDQ	6.11	0.73	6.09	5.59
MCG3	5.95	0.65	5.92	5.83

^aEnergies are in kcal/mol. D_e and D₀ are dissociation energies from the equilibrium structure and from the zero-point energy level, respectively. V[‡] is the barrier height for the hydrogen scrambling of BH₅. ^bRef. 24. ^cRef. 5. Zero-point energies are scaled by 0.95.

from frequencies calculated at the CCSD(T)/TZ2P level and scaled by 0.95. The MCCM frequencies are not scaled. If we scaled these frequencies by 0.95, the D₀ values would be increased by about 0.27 kcal/mol, and then our MCCM values agree quite well with the results by Schreiner *et al.*

The potential energy curve along the dissociation coordinate calculated at the QCISD/TZ2P, QCISD(T)//QCISD/TZ2P, CCSD(T)/cc-pVQZ//QCISD/TZ2P, and G3//QCISD/TZ2P levels are shown in Figure 1. We have plotted the potential energy with respect to the distance between B atom and the center of H₂ unit, R_c, as the dissociation coordinate. The QCISD level show unusually flat region on the potential

energy curve where R_c is between 1.6 and 2.4 Å. Using higher level of electron correlation increases the well depth and improves the shape of the curve, as shown in the curve at the QCISD(T)//QCISD/TZ2P level, but this curve is still far from the standard Morse type potential curve. At the CCSD(T)/cc-pVQZ//QCISD/TZ2P level, the potential curve is very smooth without the flat region. Not only high correlation level but also larger basis sets seems mandatory for the high quality potential energy surface. The potential energy curves plotted at the MCCM levels are shown in Figure 2. These potential curves are quite consistent with each other, and no flat region is appeared. However, these curves cannot be fitted into a single Morse type function either. It is not

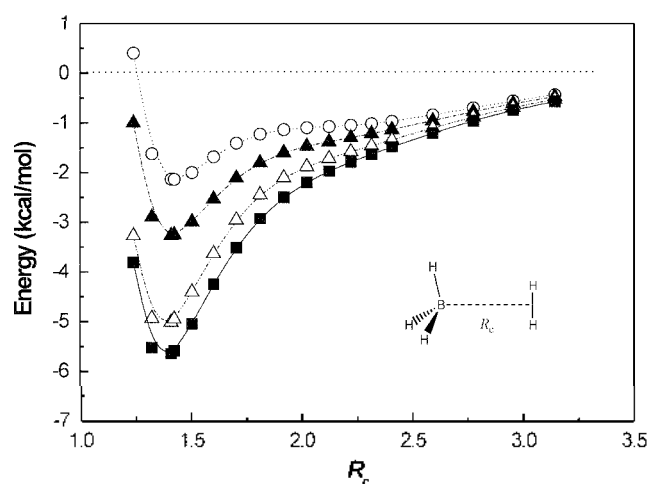


Figure 1. The potential energy curves along the dissociation coordinate of BH_3 . The partially optimized structures at the QCISD/TZ2P level were used. The open circles, closed triangles, open triangles, and closed squares are obtained at the QCISD/TZ2P, QCISD(T)//QCISD/TZ2P, G3//QCISD/TZ2P, and CCSD(T)//cc-pVQZ//QCISD/TZ2P levels, respectively.

surprising since the reaction coordinate parameter, R_c , is not defined with a single bond distance. So we made an equation with two range parameters for the Morse type function to fit the potential curves, as shown in Eq. (29).

$$V = D_e \left[[1 - a \exp\{-\alpha_1(R_c - R_e)\}] - (1 - a) \exp\{-\alpha_2(R_c - R_e)\} \right]^2 - 1 \quad (29)$$

In this equation, α_1 and α_2 are range parameters, R_e is the minimum of the potential energy curve, and α and $(1-a)$ controls the relative importance of two terms with range parameters. The estimated D_e values from Eq. (29) are listed in Table 3, and these values at the MCCM levels are almost identical to the optimized D_e values. The R_e values are 1.351, 1.351, 1.348, and 1.360 Å at the MC-QCISD, MCCM-UT-CCSD, MCCM-UT-MP4SDQ, and MCG3 levels, respectively.

Although the G3 method cannot be used to calculate the potential energy curve for the dissociation of a molecule to atomic species because of the HLC term, it is okay for BH_3 dissociation since it dissociates into two molecular species, BH_2 and H_2 . The potential curve from the G3//QCISD/TZ2P method is shown in Figure 1. This curve is better in shape than those at the QCISD or QCISD(T) levels. We have fitted the G3 potential curve to Eq. (29), and obtained 5.13 kcal/mol and 1.360 Å for the D_e and R_e values, respectively. The R_e value is the same as that from the MCG3 method, however, the D_e value is smaller than the MCCM and the CCSD(T)/TZ(3d1f1g,2p1d) values. The potential curve at the CCSD(T)/cc-pVQZ//QCISD/TZ2P level was also fitted to Eq. (29). This curve is lower in energy than the G3 curve. The well depth from the curve fitting is increased to about 5.74 kcal/mol and the R_e value is 1.366 Å. This well depth is almost identical to the D_e value at the CCSD(T)/TZ(3d1f1g,2p1d) level. These results suggest that at least the CCSD(T)/cc-pVQZ level of theory is required to generate

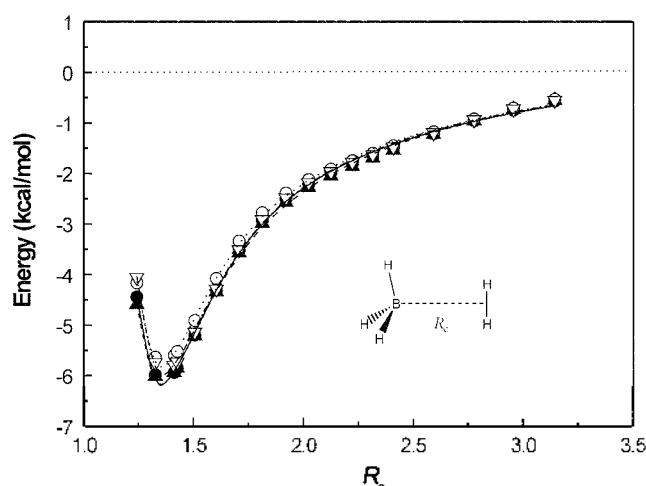


Figure 2. The potential energy curves along the dissociation coordinate of BH_3 . Potential energies were calculated by using the partially optimized structure at the QCISD/TZ2P level. The closed circles, open circles, closed triangles, and open inverted triangles are from the MC-QCISD, MCCM-UT-CCSD, MCCM-UT-MP4SDQ, and MCG3 methods, respectively. The lines passing through the point are from the best fit of Eq. (29).

reasonably accurate potential energy surface of the BH_3 dissociation.

Figure 1 and Figure 2 shows quite clearly that the MCCMs can correct the incompleteness of the QCISD level with TZ2P basis sets for the potential energy surface of BH_3 dissociation. This method is even superior to the QCISD(T)/TZ2P and G3 methods. It is interesting to note that only experimental atomization energies are used to adjust the coefficients of the MCCM. No experimental data for weak chemical interactions are used. The MCCMs have been tested successfully to reproduce the structures and energies of hydrogen-bonded dimers²¹ and hydrated proton clusters,²² and proton affinities of molecules.²³ This study and previous results suggest that the MCCM could be applied to reproduce many other chemical properties than the atomization energy. Another important observation is that the most accurate method among the MCCMs for the atomization energy is not necessarily the case for other chemical properties.²¹ In this study, all four MCCMs give almost the same results in the dissociation energy and barrier height. The Maximum deviation within these four methods is only 0.4 kcal/mol for both dissociation energy and barrier height. The MCCM-UT-CCSD agrees the best with the CCSD(T)/TZ(3d1f1g,2p1d) level.

We used the MM3 force field for the V_{11} and V_{22} terms in Eq. (7), and the MCCM-UT-CCSD method was used for energies, gradients, and Hessians for the high-level Shepard points. We defined several force field parameters for BH_3 that are missing. The potential and vibrationally adiabatic energies along the reaction coordinate are shown in Figure 3. We have used 15 high-level Shepard points step by step to generate the potential surfaces. The potential energy, V_{MEP} , is very smooth, however, the vibrationally adiabatic potential energy, V_a^3 , runs in and out slightly, along the reaction

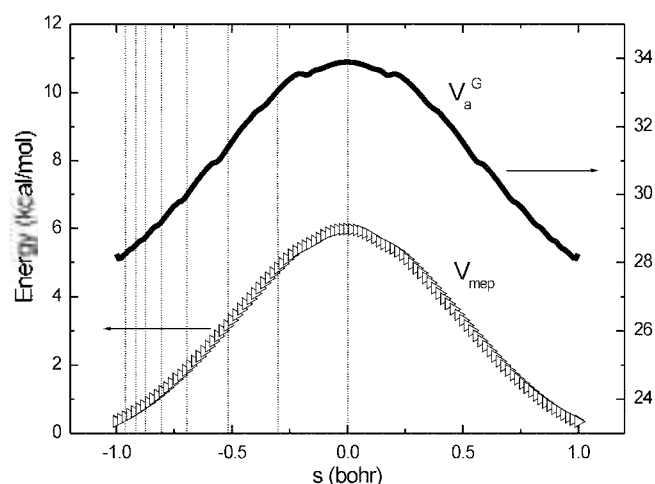


Figure 3. The potential energy and vibrational adiabatic potential energy curves along the reaction coordinate of hydrogen scrambling in BH₅. The vertical lines show the position of the high-level Shepard points at the transition state ($s=0$) and in the reactant channel ($s<0$). The same points are in the product channel ($s>0$).

coordinate. It occurs in the interpolated region between high-level Shepard points, and, in principle, it will be disappeared when we use infinite number of Shepard points. The tunneling coefficients and rate constants are listed in Tables 4 and 5. The microcannonically optimized tunneling coefficient is 7.2 at 300 K, which is large compared with the tunneling coefficient of general proton transfer reactions. The Arrhenius plots for the rate constants are shown in Figure 4. The plot for the rate constants including tunneling correction is curved; it becomes flat at a very low temperature, which indicates large tunneling effect. The rate constant at 300 K with this tunneling coefficient is $2.1 \times 10^9 \text{ s}^{-1}$, which is very fast. This suggests that the hydrogen scrambling might compete with the fast dissociation of BH₃ into BH₃ and H₂.

Table 4. Small curvature, large curvature, and microcannonically optimized tunneling coefficients at various temperatures

T (K)	$\kappa(\text{H})^{\text{SCT}}$	$\kappa(\text{H})^{\text{LCT}}$	$\kappa(\text{H})^{\text{OMT}}$
200	125	18.9	125
250	19.4	4.84	19.4
300	7.20	2.68	7.20
400	2.86	1.66	2.86
500	1.92	1.36	1.92

Table 5. Rate constants without and with tunneling corrections

T (K)	$k(\text{H})^{\text{CVT}}$	$k(\text{H})^{\text{SCT}}$	$k(\text{H})^{\text{LCT}}$	$k(\text{H})^{\text{OMT}}$
200	2.40E+06	3.00E+08	4.54E+07	3.00E+08
250	4.25E+07	8.25E+08	2.06E+08	8.25E+08
300	2.88E+08	2.08E+09	7.74E+08	2.08E+09
400	3.11E+09	8.90E+09	5.16E+09	8.90E+09
500	1.27E+10	2.45E+10	1.74E+10	2.45E+10

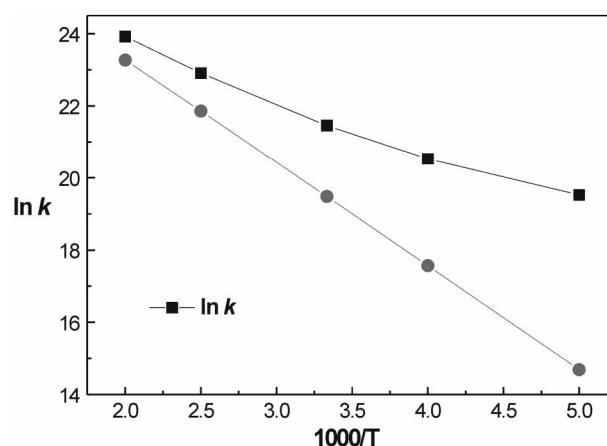


Figure 4. The Arrhenius plots for the rate constants with and without tunneling correction.

Conclusions

We have calculated structures and energies of BH₃ and the TS for the hydrogen scrambling using recently developed multi-coefficient correlated quantum mechanical methods. Our results agree very well with those from the CCSD(T)/TZ(3d1f1g,2p1d) level. We have also calculated the potential energy curves for the dissociation of BH₃ into BH₃ and H₂. The QCISD level with TZ2P basis sets produce a flat region on the potential curves, where reaction coordinate parameter, R_c , is around 1.6 and 2.4 Å. It would be necessary to use the CCSD(T)/TZ(3d1f1g,2p1d) level of theory to generate the reasonable potential energy curve for the BH₃ dissociation. The lower levels of theory were unable to give correct potential curves, whereas the MCCM generates very good potential energy curves and requires much less computing resources than the CCSD(T)/TZ(3d1f1g,2p1d) and CCSD(T)/cc-pVQZ levels.

The MCCM-UT-CCSD level of theory was used for the energy, gradients, and Hessians of high-level Shepard points, to generate the potential energy surface using the MCM algorithm. Tunneling is very important and the rate constant for the BH₃ scrambling is $2.1 \times 10^9 \text{ s}^{-1}$, which is very large. This suggests that the hydrogen scrambling might compete with the fast dissociation of BH₃ into BH₃ and H₂.

Acknowledgment. This study is supported by a grant from the Korea Research Foundation (KRF-2002-070-C00048).

References

- Mesmer, R. E.; Jolly, W. L. *Inorg. Chem.* **1962**, *1*, 608.
- Kreevoy, M. M.; Hutchins, J. E. C. *J. Am. Chem. Soc.* **1972**, *94*, 6371.
- Well, A. N.; New, J. T.; Pitzer, K. S. *J. Chem. Phys.* **1964**, *17*, 1007.
- Tague Jr., T. J.; Andrews, L. *J. Am. Chem. Soc.* **1994**, *116*, 4970.

5. Schreiner, P. R.; Schaefer, H. F.; Schleyer, P. R. *J. Chem. Phys.* **1994**, *101*, 7625.
 6. Frisch, M. J.; Trucks, G. W.; Schlegel, H. B.; Scuseria, G. E.; Robb, M. A.; Cheeseman, J. R.; Zakrzewski, V. G.; Montgomery, J. A.; Stratmann, R. E.; Burant, J. C.; Dapprich, S.; Millam, J. M.; Daniels, A. D.; Kudin, K. N.; Strain, M. C.; Farkas, O.; Tomasi, J.; Barone, V.; Cossi, M.; Cammi, R.; Mennucci, B.; Pomelli, C.; Adamo, C.; Clifford, S.; Ochterski, J.; Petersson, G. A.; Ayala, P. Y.; Cui, Q.; Morokuma, K.; Malick, D. K.; Rabuck, A. D.; Raghavachari, K.; Foresman, J. B.; Cioslowski, J.; Ortiz, J. V.; Stefanov, B. B.; Liu, G.; Liashenko, A.; Piskorz, P.; Komaromi, I.; Gomperts, R.; Martin, R. L.; Fox, D. J.; Keith, T.; Al-Laham, M. A.; Peng, C. Y.; Nanayakkara, A.; Gonzalez, C.; Challacombe, M.; Gill, P. M. W.; Johnson, B. G.; Chen, W.; Wong, M. W.; Andres, J. L.; Head-Gordon, M.; Replogle, E. S.; Pople, J. A. *Gaussian 98 Rev. A. 9*; Gaussian, Inc.: Pittsburgh, PA, 1998.
 7. Fast, P. L.; Corchado, J. C.; Sanchez, M. L.; Truhlar, D. G. *J. Phys. Chem.* **1999**, *103*, 5129.
 8. Fast, P. L.; Sanchez, M. L.; Corchado, J. C.; Truhlar, D. G. *J. Chem. Phys.* **1999**, *110*, 11679.
 9. Fast, P. L.; Sanchez, M. L.; Truhlar, D. G. *Chem. Phys. Lett.* **1999**, *306*, 407.
 10. Fast, P. L.; Corchado, J. C.; Sanchez, M. L.; Truhlar, D. G. *J. Phys. Chem. A* **1999**, *103*, 3139.
 11. Fast, P. L.; Truhlar, D. G. *J. Phys. Chem.* **2000**, *104*, 6111.
 12. Truong, T. N.; Truhlar, D. G.; Baldrige, K. K.; Gordon, M. S.; Steckler, R. *J. Chem. Phys.* **1989**, *90*, 7137.
 13. Tratz, C. M.; Fast, P. L.; Truhlar, D. G. *PhysChemComm.* **1999**, *2*, 1.
 14. Rodgers, J. M.; Lynch, B. J.; Fast, P. L.; Chuang, Y.-Y.; Pu, J.; Truhlar, D. G. *Multilevel-version 2.1.1*; University of Minnesota: Minneapolis, MN, 2000.
 15. Kim, Y.; Corchado, J. C.; Villa, J.; Xing, J.; Truhlar, D. G. *J. Chem. Phys.* **2000**, *112*, 2718.
 16. Nguyen, K. A.; Rossi, I.; Truhlar, D. G. *J. Chem. Phys.* **1995**, *5522*.
 17. Ischtwan, J.; Collins, M. *J. Chem. Phys.* **1994**, *100*, 8080.
 18. Truhlar, D. G.; Garrett, B. C. *J. Chim. Phys.* **1987**, *84*, 365.
 19. Truhlar, D. G.; Isaacson, A. D.; Garrett, B. C. In *Theory of Chemical Reaction Dynamics*, Baer, M., Ed.; CRC Press: Boca Raton, FL, 1985; Vol. 4; p 65.
 20. Garrett, B. C.; Truhlar, D. G.; Grev, R. S.; Magnuson, A. W. *J. Phys. Chem.* **1980**, *84*, 1730.
 21. Park, C.-Y.; Kim, Y.; Kim, Y. *J. Chem. Phys.* **2001**, *115*, 2926.
 22. Kim, Y.; Kim, Y. *Chem. Phys. Lett.* **2002**, *362*, 419.
 23. Seo, Y.; Kim, Y.; Kim, Y. *Chem. Phys. Lett.* **2001**, *340*, 186.
 24. Stanton, J. F.; Lipscomb, W. N.; Bartlett, R. J. *J. Am. Chem. Soc.* **1988**, *111*, 5273.
-